Point-defect interactions in electron-irradiated titanomagnetites—as analysed by magnetic

after-effect spectroscopy on annealing within 80 K < $T_a$ < 1200 K

# Point-defect interactions in electron-irradiated titanomagnetites—as analysed by magnetic after-effect spectroscopy on annealing within 80 K < $T_a$ < 1200 K

**F Walz[1], V A M Brabers[2] and H Kronmüller[1]**

[1] Max-Planck-Institut für Metallforschung, Heisenbergstraße 3, D-70569 Stuttgart, Germany
[2] Department of Physics, Eindhoven University of Technology, Potbus 513,
5600 MB Eindhoven, The Netherlands

**Abstract**
During high-temperature growing of titanomagnetite single crystals ($Fe_{2.8-\Delta}Ti_{0.2}O_4$, $\Delta < 0.005$) in oxygen enriched atmospheres, specific $Ti^{4+}$- and vacancy-based defect configurations are induced, giving rise to magnetic after-effect (MAE) spectra with peaks near 450, 200 and 65 K. The atomistic mechanisms of these relaxations are checked by exposing the crystals to low-temperature (80 K) electron ($e^-$) irradiation and subsequent analysis of the interactions between radiation-induced and lattice-inherent defects on annealing over the range $80\,K \leqslant T_a \lesssim 1200\,K$.

Within this interval, three characteristic temperature ranges are distinguished:
(a) $80\,K < T_a < 500\,K$, revealing vigorous interactions between radiation-induced and inherent defect configurations, thus demonstrating their common point-defect nature;
(b) $500\,K < T_a < 900\,K$ wherein the MAE spectra re-assume, qualitatively, their initial structure with, however, mutually modified amplitude ratios; (c) $900\,K < T_a < 1200\,K$, being characterized by the complete annihilation of all MAEs but, interestingly, also the thermally induced re-appearance of vacancies and related defect configurations.

The recovery kinetics of all prominent processes are numerically analysed and discussed with respect to their underlying atomistic mechanisms.

## 1. Introduction

The magneto-electronic properties of titanoferrites, on account of their tunability by means of appropriate Ti doping, have been under investigation for decades in various fields of applied and basic research. (i) In geomagnetics, [1–3], where titanomagnetite is frequently found as a constitutive mineral of volcanic rocks, its remanence is utilized as a 'palaeomagnetic recorder' enabling the 'play-back' of valuable information on Earth's history [4]. (ii) The magnetic characteristics of mixed ferrites like, for instance, $Mn_{1-x}Zn_xFe_2O_4$ [5]—used in various fields of electronics, telecommunications and magnetic recording [6]—were found to become considerably improved by introducing definite amounts of $Ti^{4+}$ [5, 6]. This decisive

effect of $Ti^{4+}$ doping is based on replacing two octahedrally (B)-sited $Fe^{3+}$ ions in favour of one $Ti^{4+}$ and one $Fe^{2+}$ ion, the latter one being—in contrast to $Fe^{3+}$—a carrier of both magnetic and distortional anisotropy. (iii) In magnetite research, definite doping of perfect $Fe_3O_4$ single crystals with $Ti^{4+}$—similarly as with a variety of other ions [7–9], including radiation-induced point defects like vacancies and interstitials [10]—proved to be a valuable means to clarify the atomistic mechanisms underlying both the Verwey transition (near $T_V \simeq 125\,K$) itself and the modified electronic conductivity behaviour in the temperature ranges below and above this critical temperature.

Most of the preceding work on Ti-ferrites and titanomagnetites was performed by means of non-magnetic techniques—

**Table 1.** Comparative compilation of representative activation parameters determining the typical relaxation processes in (i) zero-doped, perfectly stoichiometric magnetite single crystals, $Fe_3O_4$ (upper part of the table) and, separated by the double line, in (ii) the strongly $Ti^{4+}$-doped single-crystalline titanomagnetites ($Fe_{2.8-\Delta}Ti_{0.2}O_4$; $\Delta \simeq 0.005$) of our actual study.

| Process | $T$ (K) | $Q \pm \Delta Q$ (eV) | $\tau_0$ (s) | Mechanisms | References |
|---|---|---|---|---|---|
| $V_{1A}$ | $4 < T < 20$ | $0.03 \pm 0.02$ | $10^{-10 \pm 1}$ | Incoherent electron tunnelling | [9, 10, 13] |
| $V_{1B}$ | 30 | $0.07 \pm 0.01$ | $10^{-12 \pm 1}$ | Intra-ionic excitation (Twofold superposition) | |
| | | $0.08 \pm 0.01$ | | | |
| $V_2$ | $50 < T < 125$ | $0.25 \pm 0.10$ | $10^{-12 \pm 1}$ | Variable range electron hopping | |
| $V_{2R}$ | $\simeq 65$ | $0.17 \pm 0.04$ | $10^{-14 \pm 1}$ | $Ti^{4+}$-modified ('reversed') electron hopping | [16–18] |
| IV plateau | $150 \pm 50$ | $0.54 \pm 0.26$ | $10^{-12 \pm 1}$ | Frenkel-pair interstitial ($Fe^{2+}$) reorientation | [18] ($e^-$-irr.) |
| IV | $\simeq 200$ | $0.70 \pm 0.05$ | $10^{-14 \pm 1}$ | Intrinsic interstitial reorientation | [10, 16, 17] |
| $III_1$ | 300 | $0.85 \pm 0.05$ | $10^{-14 \pm 1}$ | B-site vacancy-mediated $Fe^{2+}$-hopping | [10, 16–18] |
| $III_2$ | | $0.93 \pm 0.05$ | | | |
| II | $\simeq 450$ | $1.24 \pm 0.15$ | $10^{-14 \pm 1}$ | Reorientation of anisotropic $Ti^{4+}Fe^{2+}$–vacancy complexes | [16–18] |

i.e. electric conductivity, heat capacity, thermoelectric power, Mössbauer effect, etc—frequently on polycrystalline samples or crystals of uncontrolled quality, as compiled in [7–9]. The latter statement holds as well for the relatively small number of preceding MAE investigations [5, 11, 12] which, moreover, suffer from the handicap of starting measurements at too elevated temperatures (i.e. 80 K, or even above the Verwey temperature), thus ignoring the most instructive low-temperature interval presenting detailed information on electronic hopping- and tunnelling-type charge transport processes [9, 13]. In view of this situation we regarded it worthwhile to resume detailed studies on single-crystalline titanomagnetites ($Fe_{3-x-\Delta}Ti_xO_4$) over a wide range of compositions ($0 \leqslant x \leqslant 1.0$; $\Delta \leqslant 0.005$) within an extended measuring interval $4\ K < T \leqslant 500\ K$, using a highly sensitive automated MAE technique.

The present report marks the final point in a series of preceding MAE studies on titanomagnetite, (a)–(d), whose topics may be summarized as informative background for the discussion of actual results.

(a) Starting from perfect single-crystalline magnetite, definite low-dose $Ti^{4+}$ doping ($0.0001 \leqslant x \leqslant 0.008$) causes systematic modification and final suppression of the initially dominating intrinsic electronic tunnelling-($4\ K < T < 25\ K$) and hopping ($50\ K < T < 125\ K$)-induced MAE processes [13], labelled as $V_{1A,B}$ and $V_2$ in table 1. This clear manifestation of elementary electron-induced MAE processes in perfect magnetite crystals points directly to low-temperature electron localization and ionic segregation—preconditions for any type of ionic ordering [9, 13, 14][3].

(b) Complementary to (a), the influence of higher $Ti^{4+}$ doping ($0.1 \leqslant x \leqslant 1$) was investigated in the system $Fe_{3-x-\Delta}Ti_xO_4$, $\Delta \simeq 0.005$, [16]. Typically, in this range all intrinsic low-temperature ($T < T_V$) electronically induced MAE processes, cf (a), are completely suppressed—except the extraordinary, sign-inverted Debye-type process near 65 K ($V_{2R}$,
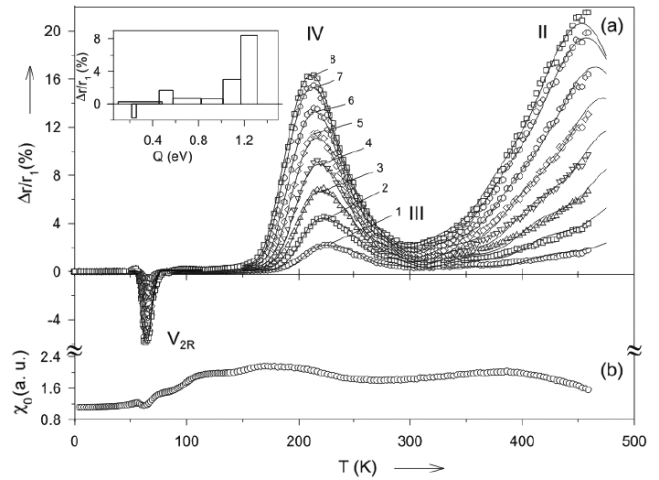


**Figure 1.** (a) Standard MAE spectrum of single-crystalline titanomagnetite with composition $Fe_{2.8-\Delta}Ti_{0.2}O_4$ ($\Delta \simeq 0.005$) in the as-grown state [16]. The various processes are conventionally indexed by roman numerals (cf table 1) and the various isochronals marked according to the times elapsed after sample demagnetization (section 2.3): i.e. $t_1 = 1$ s; (1) $t_2 = 2$, (2) 4, (3) 8, (4) 16, (5) 32, (6) 64, (7) 128 and (8) 180 s. The *experimental* data (symbols) of the various processes are *numerically fitted* (continuous lines) and their determined energy distributions—characterized by the parameters compiled in table 1, [16]—depicted in the inset. (b) Initial susceptibility of the as-grown crystal, after pre-annealing to $T_a = 500$ K. Scaling is performed in arbitrary units which, however, at 300 K correspond to an absolute value of about $\chi_0 \approx 20$—as compared to about $\chi_0 \approx 130$ in a perfect magnetite single crystal.

figure 1(a)), [16]. This process, bound to the assistance of $Ti^{4+}$-induced Jahn–Teller-like internal stresses, results from modified electron hopping, causing an *increase* instead of the usual *decrease* of the initial susceptibility. Above $T_V$, near 200 and 450 K[4], two further $Ti^{4+}$-induced relaxations arise (figure 1(a)) from reorientations of anisotropic (i) interstitial (200 K)- and (ii) complex $Ti^{4+}$–$Fe^{2+}$-vacancy (450 K)-type defect configurations. Analysis of respective relaxation strengths in dependence

---

[3] This straightforward arguing is regarded as being of such elementary urgency as to be necessarily considered in the design of any realistic magnetite model—notwithstanding contradictory conclusions derived from alternative, evidently less sensitive, techniques like, for instance, resonant x-ray scattering [15].

[4] By convenience, the basic relaxations constituting the MAE spectrum are denoted by the following, according to their positions in the initial spectrum of figure 1(a), as '65 K', '200 K' and '450 K' processes—irrespective of their actual temperature positions which, however, only in the case of the 450 K process may be notably shifted under various experimental conditions.

**Table 2.** Compilation of representative reaction parameters controlling the recovery of the basic relaxation processes in our standard titanomagnetite crystal, $Fe_{2.8-\Delta}Ti_{0.2}O_4$; $\Delta \simeq 0.005$ (figure 1(a))—as determined from kinetical analyses on the basis of least-squares fitting. Under the 'process' column the basic mechanisms of concomitant process annealing are indicated by 'Vac. Ann.'—corresponding to vacancy-induced annihilation—and 'Recomb.', corresponding to defect–anti-defect recombination.

| Process | $T_a$ (K) | $Q \pm \Delta Q$ (eV) | $K_0$ ($s^{-1}$) | $\gamma$ | Mechanisms | References |
|---|---|---|---|---|---|---|
| 450/65 Vac. Ann. | $600 < T_a < 900$ | $1.5 \pm 0.08$ | $10^{8.1\pm0.3}$ | (2) | Large-spaced Frenkel-pair recombination | Figure 3 (inset), novelty |
| 450/200 Recomb. | $900 < T_a < 1100$ | $2.45 \pm 0.03$ | $10^{8\pm0.5}$ | 2 | Vacancy—Interstitial recombination | Figures 3 and 5 [16, 17] |
| 65 | $\lesssim 1050$ | $2.45 \pm 0.05$ | $10^{8\pm0.5}$ | (2) | Breakdown of MAE-supporting stress | Figure 5 (inset), [17, 18] |
| 300/450 Vac. Ann. | $600 < T_a < 900$ | $1.40 \pm 0.1$ | $10^{8\pm0.2}$ | 2 | $Ti^{4+}$-impeded vacancy diffusion | Figure 6 [17, 18] |

of $Ti^{4+}$ doping yielded, up to $x \simeq 0.2$, preferential B-site substitution of converted 'extra $Fe^{2+}$' ions [16].

(c) The recovery behaviour of respective defect configurations was studied in detail by exposing the crystal of figure 1(a) to systematic annealing in the range $300 \text{ K} < T_a < 1200 \text{ K}$, cf table 2, [17]. The processes proved to be rather stable up to about $T_a \simeq 950 \text{ K}$, where concomitant recovery of the 450 and 200 K relaxations set in yielding, upon analysis, coincident reaction parameters of order $\gamma = 2$ and enthalpy $Q \approx 2.45$ eV. This coincidence was interpreted in terms of defect–anti-defect recombination between *vacancies*, released after thermal dissociation of 450 K complexes, and *interstitials* (200 K). The hopping-induced, stress-assisted 65 K peak undergoes delayed recovery, setting-in only in the course of stress extinction due to combined annihilation of anisotropic defect configurations.

(d) Next, we studied the effect of re-introduction of point defects—by means of low-temperature (80 K) $e^-$ irradiation—into the completely annealed crystal (c), [18]. On subsequent annealing from 80 K to $T_a \leqslant 500$ K, most radiation-induced processes are annihilated [10]— with the exception of the 65 K peak which, after resurrection near $T_a \simeq 220$ K, up to $T_A > 1000$ K, shows comparable annealing behaviour as observed in (c). Comparison between the (i) thermally(c) and (ii) radiation induced(d) spectra reveals their intimate interrelation: the pronounced 200 K peak in (i), figure 1(a), is replaced in (ii) by a broad plateau (150 K ± 50 K), corresponding to reorientations of Frenkel interstitials with a wide, perturbation-induced spectrum of activation enthalpies. Similarly, the stable 450 K process of (i) is replaced here by a pronounced maximum near 300 K, arising from reorientations of radiation-induced B-type vacancies [9, 10]. Due to their Frenkel-pair derivation, these vacancies undergo accelerated recombination with related Frenkel interstitials below $T_a \lesssim 500$ K— without any chance to form, e.g. by trapping interactions, complexes of the 450 K type.

Our actual studies may be regarded as a complementary continuation of the preceding work (d) insofar as, here, the as-produced ferrite single crystal (figure 1(a))—without any

further pretreatments—has been directly subjected to low-temperature (80 K) $e^-$ irradiation and its annealing behaviour subsequently studied in the range $80 \text{ K} \leqslant T_a \lesssim 1200 \text{ K}$. Most of the observed defect reactions compare well with the concepts developed during the preceding studies (a)–(d) so that these combined efforts represent a self-consistent contribution to our knowledge on electronic and ionic transport mechanisms in titanomagnetites.

## 2. Technical details

### 2.1. Specimen preparation

As described in more detail in the preceding study (d), [18], concerned with identically composed titanomagnetites ($Fe_{3-x-\Delta}Ti_xO_4$, $x = 0.2$, $\Delta \lesssim 0.005$), appropriately powder-sintered polycrystals were grown to $\langle 100 \rangle$-axis-oriented single crystals, using a floating zone technique [19]. Finally, these crystals were subjected to a phase-controlled tempering (during 24 h at 1473 K) and subsequent cooling-down in adjusted $CO$–$CO_2$–$H_2$ atmospheres, so as to induce a vacancy content of about $\Delta \simeq 0.005$, necessary to evoke the characteristic MAE spectrum of figure 1(a), [16, 19]. The so-produced cylindrical single crystals of about 30 mm length and 5 mm diameter were cut by spark erosion into prisms of 1.4 mm × 1.4 mm × 20 mm and, especially for $e^-$-irradiation experiments, transformed into cylinders of about 1.2 mm diameter and 10 mm length.

### 2.2. Annealing of $e^-$-irradiated specimens

In our present experiments, 'as-produced' single crystals according to section 2.1 (figure 1) have been low-temperature (80 K) $e^-$-irradiated to a dose of $\simeq 8.6 \times 10^{22} e^- \text{ m}^{-2}$ using the dynamitron accelerator of the Institut für Strahlenphysik der Universität Stuttgart. The irradiated specimens were transported and mounted into the measuring cryostat under liquid nitrogen. Recovery of MAEs was studied by annealing the samples at systematically increased temperatures, during constant time intervals of 15 min, up to temperatures of 500 K in the measuring cryostat. Annealing at higher temperatures was performed in sealed silicon–glass tubes under argon atmospheres of appropriate pressure ($\lesssim 1$ atm), in a horizontally mounted furnace with an accuracy of about

$\Delta T = \pm 2.5$ K. Annealing steps were finished by quenching the samples—within an interval of $\leqslant 5$ s to temperatures of $\leqslant 0\,^\circ$C—by either rapid cooling in the cryostat ($T_a \leqslant 500$ K) or ejection of the glass from the furnace into an ice–water bath.

### 2.3. Measuring technique

Usually our MAE data are collected—within the temperature range $4$ K $< T \leqslant 500$ K—as variations of the initial reluctivity, $r(t)$, i.e. the reciprocal of the initial susceptibility, $r(t) = 1/\chi(t)$, following axial ac sample demagnetization at highly stabilized temperatures ($\Delta T \simeq 0.01$ K). In order to determine respective susceptibility variations we apply a sensitive, low-frequency (1 kHz) LC-oscillator technique containing the crystal as core, whose eigenfrequency, via the Thomson formula, is directly related to the initial susceptibility [9, 21]. Corresponding isotherms—whose observation usually starts at $t_1 = 1$ s after sample demagnetization and continued over a standard interval of $2$ s $\leqslant t_2 \leqslant 180$ s—are transformed into the more practicable isochronal presentation, via

$$\frac{\Delta r}{r_1} = \frac{\Delta r(t_1, t_2, T)}{r(t_1, T)} = \frac{1/\chi(t_2, T) - 1/\chi(t_1, T)}{1/\chi(t_1, T)}. \quad (1)$$

This type of data presentation has the inherent advantage of immediately separating multiprocess relaxations occurring in different temperature ranges into their specific constituents, thus facilitating the numerical analysis of respective MAE spectra. This is especially true in the frequent case (as also in the actual one) that individual processes within a spectrum are characterized by exponentially activated relaxation times, $\tau = \tau_0 e^{Q/kT}$, with process parameters $Q$ (activation enthalpy), $\tau_0$ (jump time $\tau$ in the limit $T \to \infty$) and $k$ (Boltzmann constant). In such situations, by means of efficient least-squares-sum approximations, the decisive process parameters $\tau_0$, $Q$ and—in case of superimposed processes—the half-width $\Delta Q$ of respective energy spectra ($Q \pm \Delta Q$) can be determined with high accuracy [9, 21].

## 3. Experimental results

Our actual study starts with the 'as-produced' crystal of composition $Fe_{2.8-\Delta}Ti_{0.2}O_4$ ($\Delta \simeq 0.005$), cf section 2.1, being characterized by the MAE spectrum shown in figure 1(a). Without any further intermediate pretreatments, this crystal has been low-temperature (80 K) e$^-$-irradiated and, subsequently, its radiation damage annealed by systematically tempering in the range $80$ K $\leqslant T_a \leqslant 1200$ K. In addition to the original peaks near 65, 200 and 450 K, we observe after e$^-$-irradiation the emergence of two additional broad relaxation zones within $150 \pm 50$ K and about $300$ K $\pm 75$ K, resulting from superimposed relaxations of energetically varying interstitial- and vacancy-type constituents of differently spaced Frenkel pairs. The various stages of progressing crystal recovery are, in 'stroboscope-like' presentation, compiled in figure 2, out of which, for detailed inspection, the main spectral components—situated near 65 K (a), 150 K (b), 200 K (c), 300 K (d) and 450 K (e)—are extracted and combined in figure 3.
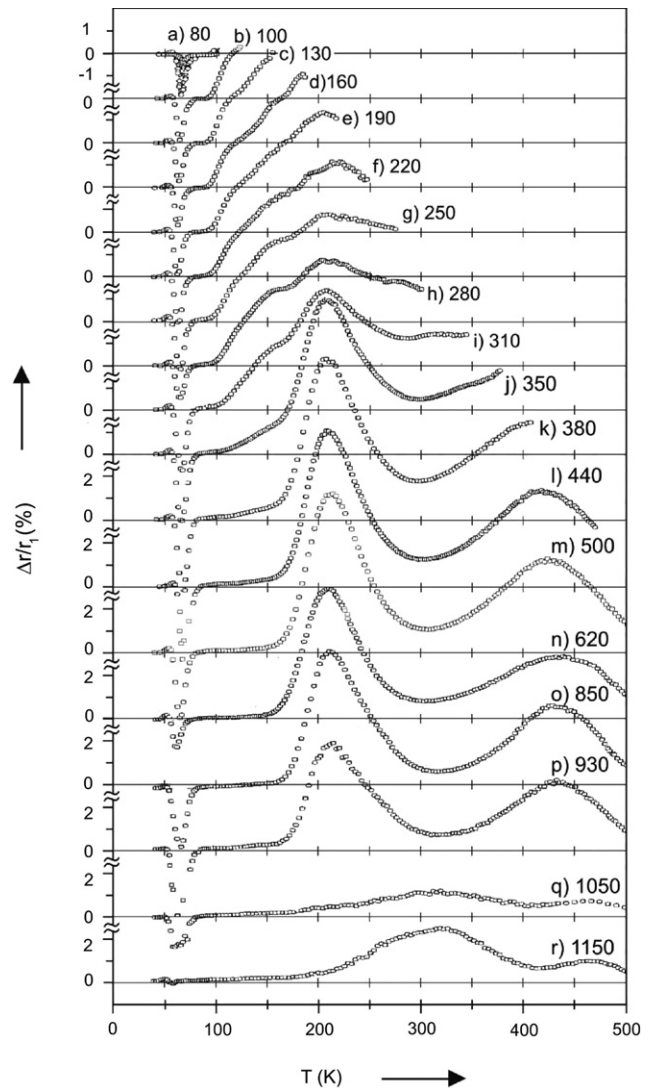


**Figure 2.** Annealing sequence, observed after low-temperature e$^-$-irradiation (section 2.2) of the crystal presented in figure 1(a). Subsequent annealing runs are marked in alphabetical order—in addition to respective annealing temperatures (in K) applied to the crystal *prior* to measurement.

Regarding the annealing behaviour over the full temperature range $80$ K $\leqslant T_a \leqslant 1200$ K, we recognize three sub-intervals of recovery, cf figures 2, 3 and table 2: (i) $80$ K $< T_a < 500$ K, within which most of the radiation-induced extra effects are annealing—thereby reconstituting qualitatively, though with varied amplitude ratios, the original spectrum: cf figures 1(a) and 2(m); (ii) $500$ K $< T_a < 950$ K, wherein, with the exception of the 65 K process (figure 3(a)), the relaxation amplitudes undergo only minor modulations; (iii) $950$ K $< T_a < 1200$ K, being characterized by the complete annihilation of processes (a) and (c)—whereas the radiation-induced component (b) had disappeared already during $T_a < 500$ K. Interestingly, such final process extinction on continued annealing is not observed for relaxation components (d) and (e) whose amplitudes—after crossing a minimum near $T_a \simeq 1050$ K—are found to re-grow again on cooling-down from higher annealing temperatures
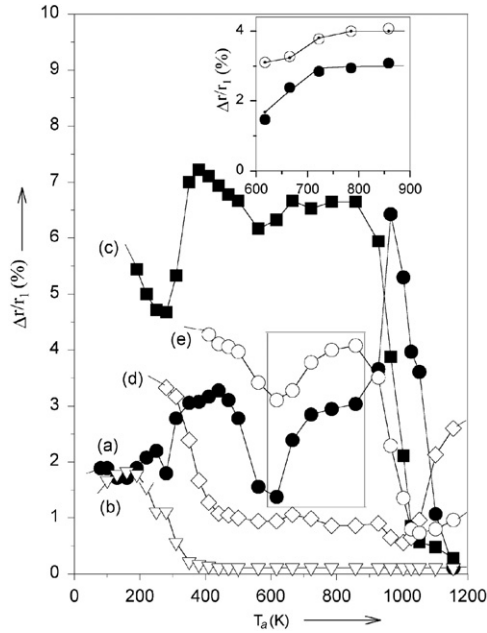
**Figure 3.** Recovery of constitutive spectral components, situated near (a) 65 K (absolute value), (b) 150 K, (c) 200 K, (d) 300 K and (e) 450 K, as traced by the peak heights ($t_2 = 180$ s) extracted from figure 2, [16, 17]. The analysis of the square-framed 450 and 65 K processes is reproduced in the, slightly scale-changed, inset.



**Figure 4.** Temperature dependences of the initial susceptibility ($\chi_0$): (i) of the as-grown crystal (cf figure 1(a)), as plotted on the in-plane diagram; (ii) effect of annealing the radiation damage on the susceptibility amplitudes at preselected temperatures (100, 200, 300 and 450 K), as plotted on the auxiliary planes, oriented at right angles to the temperature axis.

($T_a \gtrsim 1050$ K), cf figures 2(q), (r) and 3. This astonishing behaviour, already previously observed in related annealing studies [17, 18], will be further discussed in section 4.3.

　　Figure 4 gives a survey on the, relatively weak, variations of the *initial susceptibility*, $\chi_0$, in the course of a typical annealing programme. The main diagram shows the temperature dependence of $\chi_0$ over the standard measuring interval (4 K $< T \leqslant 500$ K) for the as-grown crystal, cf figures 1(a) and (b). The susceptibility $\chi_0$, expressed here in 'arbitrary units', was determined in a quantitative analysis [22] to a value of about $\chi_0 \simeq 20$ at 300 K—as compared to about $\chi_0 \simeq 130$ in perfect single crystals. For some representative measuring temperatures—i.e. $T = 100, 200, 300$ and 450 K— the annealing behaviour of the crystal susceptibility, following e⁻-irradiation, is presented over the full temperature range of annealing (80 K $\leqslant T_a \leqslant 1200$ K) on the respective, rectangularly inserted planes.

　　As described in detail in [17, 23], the activation data of prominent recovery processes were numerically determined by least-squares fitting of the recovery functions derived from the basic rate equation:

$$(\mathrm{d}c/\mathrm{d}t)_n = -c^\gamma K(T_n),$$
$$K(T_n)_{1,2} = K_{1,2}^0 \exp(-Q/kT_n),$$
(2)

with $c$ the defect concentration, expressed in terms of respective MAE amplitudes, $\gamma$ reaction order (1 or 2), $K(T)$ the reaction coefficient, expressed exponentially in terms of the activation enthalpy $Q$, annealing temperature $T_n$, Boltzmann constant $k$ and a process (order)-dependent pre-exponential factor $K_{1,2}^0$. The so-determined data of prominent recovery processes are summarized as follows, cf table 2:
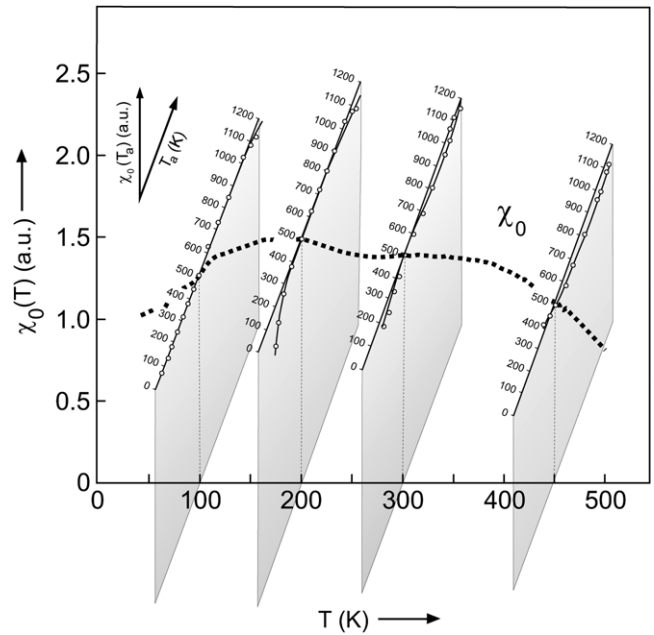
(i) Within the temperature interval 600 K $< T_A < 900$ K the strengths of the 450 and 65 K relaxations undergo considerable growth (figure 3, inset), in contrast to the other spectral components. The kinetic analysis of both growing processes yields coincident activation data of $Q = 1.5 \pm 0.08$ eV, $K_0 = 10^{8.1\pm0.3}$ s⁻¹ with undecidable reaction order between 1 and 2, cf section 4.2.

(ii) In the temperature range 950 K $< T_a < 1200$ K we observe here too, analogous to the previous annealing of the as-grown crystal (figure 1(a)) [17], concomitant recombination of the 200 and 450 K relaxation processes (cf figure 5) with coinciding reaction order $\gamma = 2$, closely related activation enthalpies of $Q = 2.43 \pm 0.05$ eV and rate constants $K_2^0 \simeq 10^{8.0\pm0.5}$ s⁻¹.

(iii) Inset (c) of figure 5 summarizes the 65 K recovery analyses of differently pretreated crystals: (i) as-grown [17]; (ii) as-grown *and* subsequently e⁻-irradiated (actual state); (iii) complete annihilation of the as-grown MAE spectrum, followed by e⁻-irradiation [18]. The determined reaction parameters agree within the limits: $Q = 2.45 \pm 0.3$ eV, $K_{1,2}^0 = 10^{8.0\pm0.3}$ s⁻¹, tending to reaction order $\gamma = 2$.

(iv) Figure 6 shows the regeneration of 300 and 450 K MAE processes which—after their first annihilation on annealing to $T_a \lesssim 1050$ K—re-appeared on quenching the crystal from elevated temperatures $T_a \gtrsim 1050$ K, cf figures 2(q), (r), 3(d) and (e). Both recovery processes obey the same set of reaction parameters: $Q = 1.40 \pm 0.1$ eV; $K_2^0 = 10^{8.0\pm0.2}$ s⁻¹; $\gamma \approx 2$, cf table 2. As discussed in the following, these results point to annealing
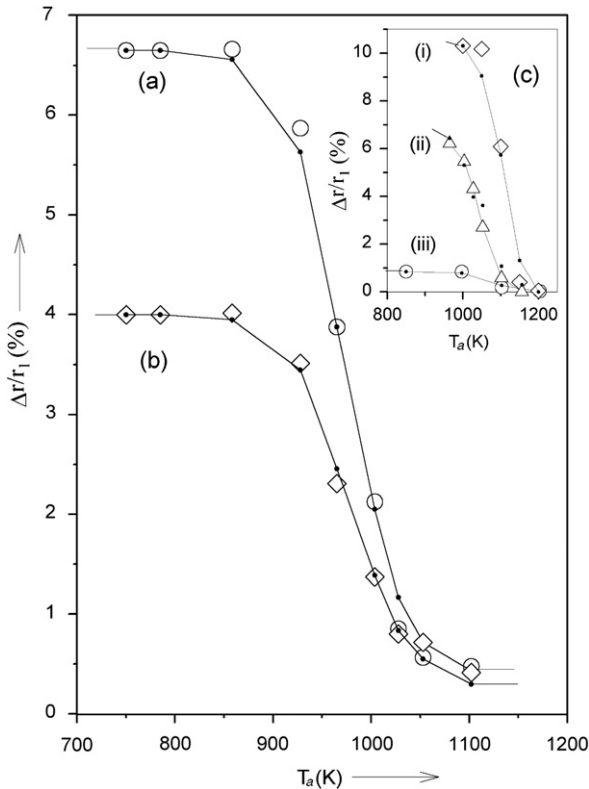
**Figure 5.** Recovery analysis of the processes situated near 200 K (a) and 450 K (b), cf figure 3, yielding coincident values of reaction order ($\gamma = 2$) and activation enthalpy ($Q \approx 2.43$ eV), cf section 3. Experimental data (symbols) are compared with their analytically determined equivalents (small points), the latter being segmentally interconnected. (c) Inset: recovery analyses of the 65 K processes (absolute values) in differently pretreated crystals: (i) as-grown [17], (ii) as-grown and subsequently $e^-$-irradiated (actual conditions); (iii) annihilation of the as-grown MAE spectrum, followed by $e^-$-irradiation, [18]. Consistent reaction parameters—e.g. $Q \approx 2.45$ eV—have been determined under the varying experimental conditions, cf section 3.
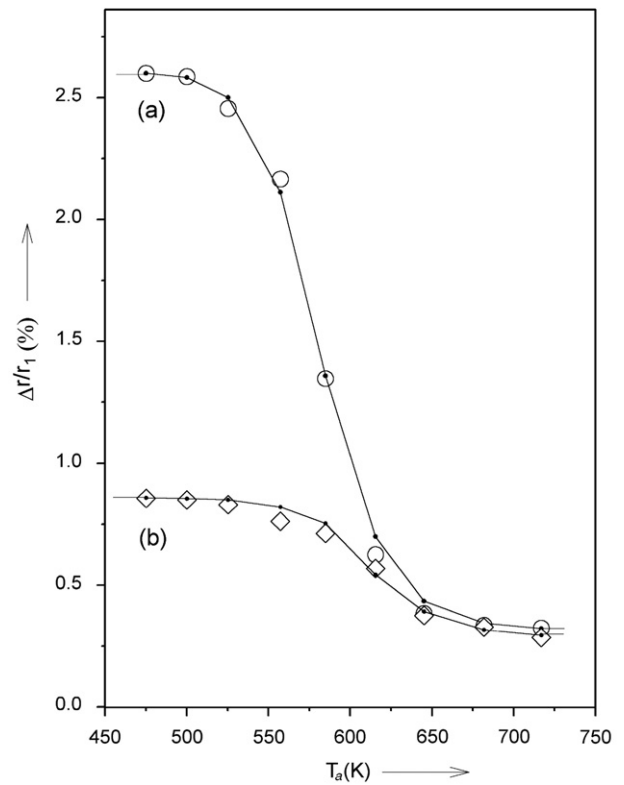


**Figure 6.** Kinetic recovery analysis of the processes re-appearing near 300 K (a) and 450 K (b), after quenching from high-temperature annealing ($T_a > 1050$ K)—yielding coincident reaction data ($Q \approx 1.40$ eV, $\gamma$ tending to 2), cf section 3; data presentation analogous to figure 5.

of both (re-developed) processes by one mobile defect, i.e. quenched-in vacancies.

## 4. Discussion

For the ease of arguing, we include in figure 7 our model conceptions as developed in preceding titanomagnetite studies [16–18] on the basis of an aptly chosen substructure of the magnetite unit cell[5]. On doping, $Ti^{4+}$ ions occupy exclusively B-type lattice sites, thereby replacing one $Fe^{3+}$ ion and transforming, for reasons of charge neutrality, one further (isotropic) $Fe^{3+}$ into an (anisotropic) $Fe^{2+}$ ion. On doping within the range of our present experiments ($x \leqslant$

0.2), the $Ti^{4+}$-induced 'extra' $Fe^{2+}$ ions are placed on B-sites, thus preserving the inverse spinel structure of the titanomagnetite [16]. For higher contents, $x > 0.2$, however, $Fe^{2+}$ ions are progressively distributed also on A-type lattice sites [16, 19]. The main lattice effect of $Ti^{4+}$ doping consists in the induction of anisotropic extra $Fe^{2+}$ ions, acting as nuclei for the formation of, i.e., $Ti^{4+}$–$Fe^{2+}$-vacancy complexes inducing the 450 K relaxation, cf section 1, figure 7(b). By cooperatively structured ordering of these local anisotropies in the single-crystalline lattice, considerable Jahn–Teller-like stresses are evoked[6], causing (i) impediment of defect reorientation as indicated by high-temperature shifting of respective peaks (450 K) [16], (ii) displacement of Fe ions into interstitial positions wherein they are inducing, by reorientations, the pronounced 200 K peak and (iii) excitation of a special mode of electron hopping (figure 7(a)) causing increasing domain wall mobility, as indicated by the sign-reversed 65 K peak, cf figure 1(a).

Following $e^-$ irradiation, various Frenkel pairs of, for example, $Fe^{2+}$, $Fe^{3+}$, $Ti^{4+}$ and $O^{2-}$ type are expected to have formed which, however—depending on formation enthalpy, anisotropy and mobility of respective defects—may have

---

[5] It may be briefly reminded here that the crystal structure of perfect magnetite is of inverse spinel type, described by the formula $Fe^{3+}[Fe^{3+}Fe^{2+}]O_4$, corresponding to a unit cell composed of 32 close (fcc) packed $O^{2-}$ ions comprising 64 tetrahedral (A-type) and 32 octahedral (B-type) interstices [9]. Typically, the tetrahedral sublattice is occupied by one octet of $Fe^{3+}$ ions, whereas the octahedral sublattice (indicated by squared brackets) is inhabited by two octets of, respectively, $Fe^{3+}$ and $Fe^{2+}$ ions.

[6] The effect of continued $Ti^{4+}$ doping on the crystal anisotropy, especially in the case of preponderant A-site occupation of displaced extra $Fe^{2+}$ ions, is described in more detail in [16, 19, 24]. Thus, the final composition of Ulvö-spinel ($Fe_2TiO_4$) is characterized by pronounced Jahn–Teller distortions, connected with giant magnetostriction.
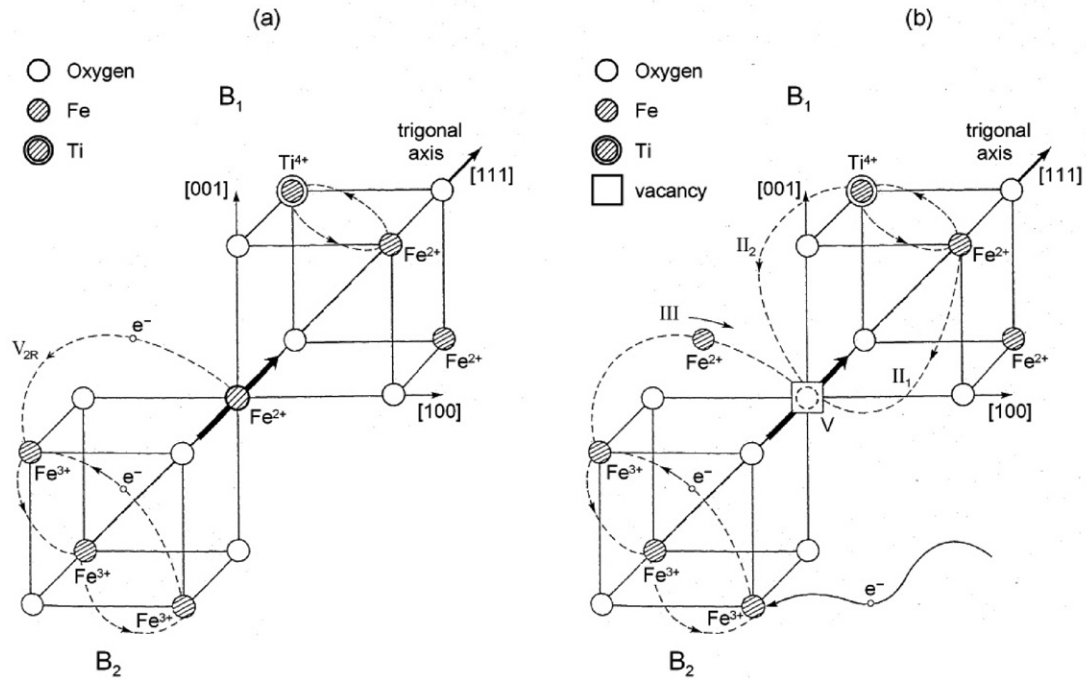
**Figure 7.** (a) Elementary B-site configuration of the inverse spinel lattice, illustrating stress reduction around $B_1$ by electron jumping from the $Ti^{4+}$-distorted minicube $B_1$ into $B_2$ ($V_{2R}$, figure 1(a)). By a sequence of such jumps, anisotropy transport from, for example, the interior to the periphery of the domain wall is feasible, thus boosting the wall mobility around $B_1$ [16, 17]. (b) Model of the 450 K relaxation process (figure 1(a)) in terms of $Fe^{2+}Ti^{4+}$-pair—vacancy complexes, formed during high-temperature crystal annealing. By jumping of a bound $Fe^{2+}(II_1)$ or $Ti^{4+}(II_2)$ ion into the vacancy (V), the local anisotropy of the complex is reoriented, thus inducing the characteristic relaxation near 450 K [16, 17], cf table 1.

a different impact on the observed MAE spectra. Since formation and migration enthalpies of Frenkel defects are supposed to increase in proportion to the valence and diameter of engaged ions [18], B-type Frenkel defects are expected to be of major influence on the observed MAE spectra. Accordingly, Frenkel defects of higher formation enthalpies are supposed to form closer pairs, undergoing faster recombination on thermal annealing, than larger distance pairs endowed with lower formation enthalpies.

### 4.1. Defect reactions on annealing in the interval $80\,K \lesssim T_A \lesssim 500\,K$

On inspection of the induced radiation damage, as resolved in the course of systematic annealing, cf figures 2 and 3, we recognize first an only moderately attenuated 65 K peak. This is followed by a bilateral superimposition of the surviving 200 K peak by two broad relaxation wings extending, respectively, within $150 \pm 50$ K and $300$ K $\pm$ 75 K. In terms of our previous arguing [18], these wings are associated with distributions of variably dissociated Frenkel pairs whose interstitial- and vacancy-type partners undergo combined reorientation and annihilation within a spectrum of activation enthalpies, figures 3(d) and (b). The further annealing up to $T_a \leqslant 500$ K is characterized by (i) complete annihilation of the two extended wings—leaving back a minor, already initially existing background relaxation around

300 K (figure 1(a)) and (ii) re-appearance of the 450 K peak, accompanied by steady growth of the 65 and 200 K peaks being related to progressing annihilation of radiation-induced lattice perturbations impeding, initially, the relaxation of pre-existing defect configurations.

Additional information on the nature and relaxation mechanisms of participating defects is obtained by comparing temperature positions and amplitude relations of respective processes in (i) un-irradiated (figure 1(a)) and (ii) $e^-$-irradiated, subsequently to 500 K annealed (figure 2(m)), crystals. Thus, fair agreement is observed for the temperature positions of the 65, 200 and 300 K relaxations—where the latter, vacancy-induced process is reduced, at the actual $Ti^{4+}$ content, to a minor background relaxation [16, 17]. In contrast to this agreement, however, the peak situated prior to irradiation near 450 K, after irradiation and annealing to $T_a = 500$ K, has shifted to a lower temperature of about 425 K, cf figures 2(l)–(p). Regarding the relations of normalized amplitudes, $A(T)/A(65\,K)$, between respective peaks of the two differently pretreated crystals (i) and (ii), the following values are obtained— **u** and **e** denoting the un-irradiated and $e^-$-irradiated crystal state, respectively:

$$[A(65\,K){:}A(200\,K){:}A(300\,K){:}A(450\,K)]/A(65\,K)$$

$$= \begin{cases} \mathbf{u}: & 1{:}2.7{:}0.38{:}3.6 \\ \mathbf{e}: & 1{:}2.4{:}0.36{:}1.4. \end{cases} \tag{3}$$

The fundamental nature of the striking discrepancy between the 450 K peak heights in the crystal states **u** and **e** is further stressed by the fact that, over the whole annealing range (80 K < $T_a$ < 1200 K), in crystal 'u' the amplitude of the 450 K process outweighs by far the one of the 200 K process (figure 1(a)), in contrast to the situation in crystal 'e', where the reverse is true (figures 2(l)–(m)), [16, 17]. This finding, in combination with the annealing behaviour of the 65 K process [17, 18], is a clear indication that—on annealing to $T_a$ = 500 K—the induced radiation damage has not recovered by only a simple defect–anti-defect recombination. Rather, the induced point defects are participating also in interactions with pre-existing, growth-generated defects and in the formation of further defect configurations which—though remaining immobile within our observation range (4 K < $T$ ⩽ 500 K)—are diagnosable from specific characteristics of the 65 K MAE.

### 4.2. Defect reactions on annealing in the interval $500\,K \lesssim T_A \lesssim 900\,K$

(a) On annealing to about $T_a$ ≃ 500 K, the amplitudes of the 65 and 200 K processes surpass two correlated maxima (figures 3(a) and (c)), whereas the 450 K process decreases, from its first appearance, attaining a minimum near 600 K (figure 3(e)). The former two maxima result from a superposition of two counteracting processes during annealing: (i) increasing strength, due to elimination of relaxation-impeding lattice damages and (ii) decrease of strength, due to annihilation of corresponding relaxators (200 K) together with their associated internal stresses, thus causing diminution of the 65 K process. With the onset of vacancy mobility, near $T_a$ ≈ 300 K, the initially growth-induced interstitials, too, become increasingly annihilated, thus further attenuating the 200 K and, consequently, the 65 K peak—down to a minimum near 600 K, being common also to the 450 K process, cf figures 3(a), (c) and (e). The decrease of the latter process, on annealing in the interval 400 K < $T_a$ < 600 K, is associated with a destabilization of respective $Ti^{4+}$–$Fe^{2+}$-vacancy complexes due to interactions with still present, thermally activated vacancies.

(b) The subsequent recovery of the 450 K process, on annealing within 600 K < $T_a$ < 900 K (cf figures 3(a) and (e) with inset), is tentatively assigned to a mobilization of radiation-induced distant Frenkel pairs of $Fe^{2+}$ and/or $Ti^{4+}$ type. In the course of these defect reactions— being compatible with corresponding tracer diffusion results [25–27]—renewed formation of anisotropic 450 K complexes, as indicated by a rise of respective MAE amplitudes, appears feasible. Due to the herewith increasing number of local stress centres, in terms of the developed picture, a corresponding growth of the 65 K process is expected as a natural consequence.

### 4.3. Defect reactions on annealing in the interval $900\,K \lesssim T_A \lesssim 1200\,K$

As shown in figures 2 and 3, within this relatively narrow temperature range all, so far surviving, components of the

MAE spectrum are rapidly annihilating. From the fact that after annealing to 500 K the original MAE spectrum has been qualitatively re-established in the $e^-$-irradiated crystal, it appears plausible that the reaction parameters of respective processes determined from actual analyses compare well those obtained previously for the unirradiated crystal (section 3), [17]. This leads us to interpret our present observations in agreement with previously established concepts as follows [17, 18], cf table 2:

(a) The thermal activation data of the 200 and 450 K processes (section 3), and especially their concomitant second-order recovery, point to a mutual defect–anti-defect recombination, cf figures 3 and 5. This reaction is most likely to occur between $Ti^{4+}$-induced $Fe^{2+}$ interstitials and B-site vacancies, the latter becoming released by dissociation of anisotropic $Fe^{2+}Ti^{4+}$-vacancy complexes, cf figure 7(b). The relatively high recovery enthalpy of 2.45 eV—as compared with the lower relaxation enthalpies of 0.7 eV (200 K process) and 1.24 eV (450 K process)—underlines (i) the high stability of these complexes and reveals (ii) their 'caged' reorientation mode around an immobile (non-diffusing) mass centre of respective defect configurations. Presumably, dissociation of these complexes is associated with the onset of thermal vacancy formation, cf (c), whose activation enthalpy is reported, from tracer diffusion in comparable titanomagnetites, to be of the order ≲2.65 eV, [27]. The thereupon envisaged release of vacancies from their destabilized complexes has a dual effect on the MAE spectrum: (i) elimination of the 200 K relaxation by recombination of highly mobilized vacancies (due to their relatively low activation enthalpy of 0.9 eV < $Q_V$ < 1, 4 eV [17, 26], table 1) and interstitials, in addition to (ii) immobilization (suppression) of the 450 K relaxation by the, diffusion-specific [9], replacement of the MAE-supporting vacancy (V, figure 7(b)) by an $Fe^{2+}$ ion.

(b) The recovery curve of the 65 K process within the range 900 K < $T_a$ < 1200 K is characterized by the appearance of a pronounced maximum after annealing near 950 K, cf figure 3(a). Again, two counteracting effects are regarded to be responsible for this phenomenon: (i) activation of an increasing number of 65 K relaxators (cf figure 7(a)), re-established in the course of lattice recovery near $T_a$ < 1000 K and (ii) a concomitant decrease of Jahn–Teller like lattice stresses—due to the breakdown of anisotropic defect configurations—thus causing attenuation of the stress-sensitive 65 K relaxation at $T_a$ > 1000 K. Finally, at temperatures above 1100 K —with the vanishing of all defect-induced anisotropies and their correlated stresses— the 65 K process, too, is breaking down, cf figures 2 and 3.

(c) An interesting phenomenon is the re-appearance of the—intermediately almost completely annealed—300 and 450 K relaxations on quenching from temperatures $T_a$ ≳ 1100 K. In terms of a vacancy formation enthalpy of about 2.45 eV (cf (a), section 3), these renewed processes are interpreted as local anisotropy reorientations due to (i) migration of B-type vacancies

(300 K) and (ii) reorientations of a minor number of re-created 450 K complexes. The concomitant recovery of these processes, following an activation enthalpy of about 1.4 eV (section 3, figure 5), is attributed to the onset of vacancy diffusion near $T_a \gtrsim 550$ K, ending in the dissolution of not yet stabilized $Ti^{4+}$–$Fe^{2+}$-vacancy complexes, and vacancy precipitation at peripheral sinks. The measured, increased vacancy migration enthalpies of this order—$Q_V \approx 1.4$ eV, instead of $Q_V \simeq 0.9$ eV in impurity-free magnetite—are in agreement with tracer diffusion experiments in titanomagnetites of similar compositions, cf [17, 25–27], being associated with the $Ti^{4+}$-induced impediment of defect mobility [16].

## 5. Summary

(1) Marking the endpoint of a series of MAE studies on titanomagnetites under various experimental conditions [13, 16–18], this paper is concerned with the radiation damage, introduced by low-temperature (80 K) $e^-$ irradiation, into a single crystal of composition $Fe_{2.8-\Delta}Ti_{0.2}O_4$, $\Delta < 0.005$. Crystals of this type, in the as-grown state, are characterized by three pronounced relaxation maxima situated near 450, 200 and 65 K, being associated, respectively, with reorientations of anisotropic $Ti^{4+}$–$Fe^{2+}$-vacancy complexes, $Fe^{2+}$-type interstitials and a so far unknown, striking form of electron hopping, causing an *increase*, instead of the usually observed *decrease*, of the initial susceptibility.

(2) The effect of $e^-$ irradiation on such as-grown crystals consists essentially in a superposition of the original MAE spectrum by additional, radiation-induced relaxation processes—identified as resulting from a variety of close and distant Frenkel pairs—contributing to the MAE spectra with reorientation-type (interstitials) and diffusion-like (vacancies) processes. On annealing to $T_a \lesssim 500$ K, with the qualitative re-appearance of the standard MAE spectrum, all radiation damage in the crystal seems to have recovered again—similarly as in the case of $e^-$-irradiated perfect magnetite single crystals [10].

(3) Thorough inspection of the restored MAE spectrum reveals, however, considerably changed amplitude relations as compared to the pre-irradiated crystal state—especially concerning the 450 K process. This observation points to incomplete recombination of radiation-induced defects due to, for example, formation of new defect configurations, by either self-trapping and/or trapping at inherent lattice defects. Although these reaction products, themselves, remain invisible—due to a lack of thermal activation within our measuring interval (4 K < $T \leqslant 500$ K)—the assumption of their existence appears, nevertheless, stringent and crucial for the understanding of the relaxation and annealing mechanisms of the 65 K process.

(4) Despite the occurrence of modified amplitude ratios in radiation-annealed crystals, respective spectral components undergo analogue recovery kinetics as in un-irradiated, identically composed crystals [17]: again,

the 200 and 500 K processes recover in terms of a bimolecular reaction ($\gamma = 2$) with an activation enthalpy of about $Q \simeq 2.45$ eV—necessary in this order to release bound vacancies which, subsequently, recombine with interstitials. The 65 K process—representing one of the rare examples displaying inverse MAE relaxation [20-(1984)], discovered in our experiments to be of extreme stress sensitivity—is the last of the basic relaxations to annihilate at $T_a \gtrsim 1100$ K, i.e. in a range where all other anisotropic defect configurations—together with their adjoint local stress contributions—have already disappeared.

## References

[1] Nagata T 1961 *Rock Magnetism* (Tokyo: Maruzen)
[2] Gubbins D and Herrero-Bervera F (ed) 2007 *Encyclopedia of Geomagnetism and Paleomagnetism* (Dordrecht: Springer)
[3] Butler R 1992 *Paleomagnetism: Magnetic Domains to Geologic Terranes* (Boston, MA: Blackwell)
[4] Kosterov A 2007 *Encyclopedia of Geomagnetism and Paleomagnetism* (Dordrecht: Springer) p 515
[5] Knowles J E 1974 *Phil. Res. Rep.* **29** 93
[6] Enz U 1982 *Ferromagnetic Materials* vol 3, ed E P Wohlfarth (Amsterdam: North-Holland) p 3
[7] Brabers V A M 1995 *Handbook of Magnetic Materials* vol 8, ed K H Buschow (Amsterdam: Elsevier Science) p 189
[8] Honig J M 1995 *J. Alloys Compounds* **229** 24
[9] Walz F 2002 *J. Phys.: Condens. Matter* **14** R285
[10] Walz F and Kronmüller H 1990 *Phys. Status Solidi* b **160** 661
    Walz F and Kronmüller H 1994 *Phys. Status Solidi* b **181** 485
[11] Höhne R, Melzer K, Hochschild H, Libor G and Krause R 1975 *Phys. Status Solidi* a **27** K117
[12] Schmidbauer E and Fassbinder J 1987 *J. Magn. Magn. Mater.* **68** 83
[13] Walz F, Brabers V A M, Brabers J H V J and Kronmüller H 2005 *J. Phys.: Condens. Matter* **17** 6763
[14] Fähnle M, Kronmüller H and Walz F 2005 *Physica* B **369** 177
[15] Garcia J and Subias G 2004 *J. Phys.: Condens. Matter* **16** R145
[16] Walz F, Brabers V A M, Brabers J H V J and Kronmüller H 2003 *J. Phys.: Condens. Matter* **15** 7029
[17] Walz F, Brabers V A M, Brabers J H V J and Kronmüller H 2007 *Phys. Status Solidi* a **204** 3514
[18] Walz F, Brabers V A M and Kronmüller H 2008 *Phys. Status Solidi* a **205** 2934
[19] Brabers V A M 1995 *Physica* B **205** 143
[20] Walz F 1971 *Phys. Status Solidi* a **8** 125
    Walz F 1974 *Appl. Phys.* **3** 313
    Walz F 1984 *Phys. Status Solidi* a **82** 179
    Walz F 1995 *Phys. Status Solidi* a **147** 237
[21] Blythe H J, Kronmüller H, Seeger A and Walz F 2000 *Phys. Status Solidi* a **181** 233
[22] Walz F, Weller M and Hirscher M 1996 *Phys. Status Solidi* a **154** 765
[23] Walz F, Wakisaka T and Kronmüller H 2005 *Phys. Status Solidi* a **202** 2667
[24] Kataoka M 1974 *J. Phys. Japan* **36** 456
[25] Aragon R, McCallister R H and Harrison H R 1984 *Contrib. Mineral. Petrol.* **85** 174
[26] Dieckmann R and Schmalzried H 1986 *Ber. Bunsenges. Phys. Chem.* **90** 564
[27] Aggarwal S and Dieckmann R 2002 *Phys. Chem. Miner.* **29** 707